On the Role of the Helmholtz Decomposition in Mixed Methods for Incompressible Flows and a New Variational Crime

A. Linke [1]

Abstract

According to the Helmholtz decomposition, the irrotational parts of the momentum balance equations of the incompressible Navier-Stokes equations are balanced by the pressure gradient. Unfortunately, nearly all mixed methods for incompressible flows violate this fundamental property, resulting in the well-known numerical instability of poor mass conservation. The origin of this problem is the lack of L^2-orthogonality between discretely divergence-free velocities and irrotational vector fields. In order to cure this, a new variational crime using divergence-free velocity reconstructions is proposed. Applying lowest order Raviart-Thomas velocity reconstructions to the nonconforming Crouzeix-Raviart element allows to construct a cheap flow discretization for general 2d and 3d simplex meshes that possesses the same advantageous robustness properties like divergence-free flow solvers. In the Stokes case, optimal a-priori error estimates for the velocity gradients and the pressure are derived. Moreover, the discrete velocity is independent of the continuous pressure. Several detailed linear and nonlinear numerical examples illustrate the theoretical findings.

Keywords: mixed finite elements, incompressible Navier-Stokes equations, divergence-free methods, Helmholtz decomposition, poor mass conservation

1. Introduction

In the last forty years mixed finite elements for the incompressible Navier-Stokes equations have seen a great success in mathematical fluid dynamics [30, 8, 43, 18, 33, 16]. The theory of mixed finite elements is elegant and compact, and it delivers rather simple recipes for the construction of convergent numerical schemes with easily predictable convergence rates and other distinctive properties. Obviously, the great flexibility of mixed finite elements is mainly indebted to the relaxation of the divergence constraint [8, 31]. However, there is a price to pay for this relaxation. This price can be observed most easily from the typical a-priori mixed finite element estimate

for the incompressible Stokes equations

$$\begin{aligned} -\nu\Delta\mathbf{u} + \nabla p &= \mathbf{f}, && \mathbf{x} \in \Omega, \\ -\nabla \cdot \mathbf{u} &= 0, && \mathbf{x} \in \Omega, \\ \mathbf{u} &= \mathbf{0}, && \mathbf{x} \in \partial\Omega \end{aligned} \tag{1}$$

that reads as

$$\|\mathbf{u} - \mathbf{u}_h\|_{1,h} \leq C_1 h^k |\mathbf{u}|_{k+1} + \frac{C_2}{\nu} h^k |p|_k, \tag{2}$$

emplyoing finite elements of polynomial order k for the discrete velocities and finite elements of order $k-1$ for the discrete pressure [8, 30, 43]. Here, the price consists in the error term $\frac{C_2}{\nu} h^k |p|_k$, which is classical for *exterior*, i.e., non-divergence-free, mixed methods in the sense of Ref. [30], but links the discrete velocity $\mathbf{u}_h$ in a disadvantageous manner with the continuous pressure p. This price, which by the way can be avoided completely by divergence-free mixed methods like the classical Scott-Vogelius element[49, 48, 41, 51] or more recent divergence-free discretization approaches[11, 12, 50, 20, 21, 22], is well-known in the finite element community as poor mass conservation [36, 35]. In mixed finite elements it is traditionally tried to get around with poor mass conservation by stabilization techniques like grad-div stabilization[23, 43, 40, 39, 34, 27, 5, 10, 38] or by variable transformations reducing the complexity of the continuous pressure[26, 47]. An interesting, alternative approach in the Stokes case was proposed in [28], employing a (discrete) Helmholtz decomposition of the exterior forcing. But these techniques always seem to mitigate this problem only, are restricted to special cases and never solve it completely[25, 32]. But although poor mass conservation has accompanied the development of mixed methods for incompressible flows for several decades, surprisingly only in recent years research on poor mass conservation began to receive a broader attention and a better understanding of it started [40, 39, 9, 35, 36, 25, 10, 37].

Nowadays, it is clear that poor mass conservation is resonsible for several different kinds of non-physical behaviour that is shown by (exterior) mixed methods for incompressible flows. As a nice example, the observations by Dorok et al. are mentioned here, which are already several years old [17]. There, the authors show that in a heated cavity flow a change of the absolute values of some inhomogeneous Dirichlet boundary conditions for the temperature changes the discrete velocity field, although in the continuous counterpart only the difference between the different temperatures matters. The reason for this strange behavior of *exterior* mixed methods roots in a (discrete) violation of a fundamental invariance property of the (continuous) incompressible Navier-Stokes equations (with homogeneous Dirichlet boundary conditions). Changing the exterior forcing by $\mathbf{f} \to \mathbf{f} + \nabla\psi$, changes the Navier-Stokes solution by $(\mathbf{u}, p) \to (\mathbf{u}, p + \psi)$, i.e., the velocity does not change and the additional forcing is balanced by the

pressure gradient. In Dorok et al. [17], it is nicely explained that in their heated cavity problem a change of the absolute temperature level induces an additional irrotational buoyancy term that is is treated in a non-physical way by exterior mixed methods. Continuing this discussion, one should note that there is an important special case of the fundamental invariance property of incompressible flows above, where exterior mixed methods can collapse dramatically. This special case occurs, whenever the forcing $\mathbf{f}$ is completely irrotational, i.e., $\mathbf{f} \equiv \nabla\psi$. In such cases, the forcing does not excite any motion in a fluid, but exterior mixed methods usually suffer from large spurious velocity oscillations, which have been observed in the past by several works [28, 17, 24, 35, 10]. Another example of non-physical poor mass conservation is visible, when the Coriolis force is added to the incompressible Navier-Stokes equations. Since the Coriolis force $2\,\Omega \times \mathbf{u}$ may have a large irrotational part in the sense of the Helmholtz decomposition in some physical situations (e.g., in two dimensions, the Coriolis force is always irrotational [14] !), it excites spurious velocity oscillations [14, 13], since discretely divergence-free velocity fields in exterior mixed methods are not orthogonal to this irrotational forcing in the L^2 scalar product. A very similar, well-known example is the rotational form of the incompressible Navier-Stokes equations [34], where the nonlinear term $(\mathbf{u}\cdot\nabla)\mathbf{u}$ is replaced by $\omega \times \mathbf{u}$ with $\omega = \nabla \times \mathbf{u}$. Here, exterior mixed methods deliver different, usually remarkably worse discrete velocity fields compared to discretizations employing the nonlinear term $(\mathbf{u}\cdot\nabla)\mathbf{u}$, although the corresponding continuous velocity fields are the same [34, 4]. In the numerical section of this contribution, it will be shown how an inappropriate treatment of the (large) irrotational part of the nonlinear term $\omega \times \mathbf{u}$ is responsible for poor accuray in simulations.

Therefore, it has recently been pointed out that poor mass conservation is maybe a misleading term, and could be described probably better by a kind of poor momentum balance, resulting from a lack of L^2-orthogonality between irrotational and discretely-divergence-free vector fields [37]. Following these ideas, in this contribution the significance of the *continuous* Helmholtz decomposition in discretizations of incompressible fluids is emphasized, and a new kind of variational crime is introduced, in order to cure the lack of L^2-orthogonality between irrotational and discretely divergence-free vector fields. Thereby, a simple, cheap and robust lowest-order discretization for the incompressible Navier-Stokes will be constructed on regular simplex grids in two and three space dimensions, which is based on the classical nonconforming Crouzeix-Raviart element [15, 3, 1]. Here, the variational crime consists in replacing discretely divergence-free vector fields by divergence-free lowest-order Raviart-Thomas [42, 8, 19] velocity reconstructions, wherever L^2 scalar products occur in the momentum balance equations. The motivation behind this discretization approach will be explained in detail in the next section. Last but not least, it should be noted that the up-to-

now rare use of divergence-free Navier-Stokes discretizations in practice is probably mainly indebted to their expensive costs even on coarse meshes and too severe constraints on the used triangulations. Therefore, the variational crime proposed in this contribution could be a viable resort out of this dilemma.

The contribution is organized as follows. The new finite element method based on Raviart-Thomas velocity reconstructions for the nonconforming Crouzeix-Raviart element will be presented in Section 3. In Section 4, a-priori error estimates for the incompressible Stokes equations are derived. Especially, the estimates for the discrete velocity are completely independent of the continuous pressure, like in divergence-free methods [35]. In Section 5, detailed numerical examples show the robustness and acuracy of the proposed scheme. Here, the emphasis is on avoiding poor mass conservation in the *left hand side* of the momentum balance equations, which is the harder problem to solve. Especially, it will be demonstrated that the rotational form of the incompressible Navier-Stokes equations can be safely used, if appropriate velocity reconstructions are applied.

2. Continuous Setting, Some Mathematical Background and the Helmholtz Decomposition

As a model problem, we investigate the steady incompressible Navier-Stokes equations with homogeneous Dirichlet boundary conditions that read as

$$\begin{aligned} -\nu\Delta\mathbf{u} + (\mathbf{u}\cdot\nabla)\,\mathbf{u} + \nabla p &= \mathbf{f}, && \mathbf{x}\in\Omega, \\ -\nabla\cdot\mathbf{u} &= 0, && \mathbf{x}\in\Omega, \\ \mathbf{u} &= \mathbf{0}, && \mathbf{x}\in\partial\Omega. \end{aligned} \tag{3}$$

These equations are posed in a polyhedral, simply-connected domain $\Omega\subset\mathbb{R}^d$ with $d\in\{2,3\}$, and it is searched for the velocity field $\mathbf{u}$ and the pressure p. Introducing $X = H_0^1(\Omega)^d$ and $Q = L_0^2(\Omega)$, a weak formulation of this problem is given by [46]: search for $(\mathbf{u},p)\in X\times Q$ such that for all $(\mathbf{v},q)\in X\times Q$ holds

$$\begin{aligned} a(\mathbf{u},\mathbf{v}) + c(\mathbf{u},\mathbf{u},\mathbf{v}) + b(\mathbf{v},p) &= l(\mathbf{v}), \\ b(\mathbf{u},q) &= 0. \end{aligned} \tag{4}$$

Here, $a : X\times X\to\mathbb{R}$, and $b : X\times Q\to\mathbb{R}$ are continuous bilinear forms, $c : X\times X\times X :\to\mathbb{R}$ is a continuous trilinear form, and $l : X\to\mathbb{R}$ is a

continuous linear form. All these forms are given by

$$\begin{aligned} a(\mathbf{u},\mathbf{v}) &:= \nu \int_\Omega \nabla\mathbf{u} : \nabla\mathbf{v}\, dx, \\ b(\mathbf{u},q) &:= -\int_\Omega q\nabla\cdot\mathbf{u} dx, \\ c(\mathbf{a},\mathbf{u},\mathbf{v}) &:= \int_\Omega ((\mathbf{a}\cdot\nabla)\,\mathbf{u})\cdot\mathbf{v}\, dx, \\ l(\mathbf{v}) &:= \int_\Omega \mathbf{f}\cdot\mathbf{v}\, dx. \end{aligned} \tag{5}$$

Introducing the space of weakly differentiable, divergence-free functions

$$V := \{\mathbf{v}\in X : \nabla\cdot\mathbf{v} = 0\}, \tag{6}$$

one can also formulate the saddle point problem (4) as an elliptic one for the velocity alone, i.e., we search for $\mathbf{u}\in V$ such that

$$a(\mathbf{u},\mathbf{v}) + c(\mathbf{u},\mathbf{u},\mathbf{v}) = l(\mathbf{v}) \tag{7}$$

holds for all $\mathbf{v}\in V$. This elliptic problem defines the velocity solution completely [46]. Introducing the orthogonal complement of V with respect to the scalar product $(\nabla\mathbf{u},\nabla\mathbf{v})$ by

$$V^\perp := \{\mathbf{v}\in X : \forall\mathbf{w}\in V : a(v,w) = 0\}, \tag{8}$$

one obtains an additional set of equations solving for the pressure: for all $\mathbf{v}\in V^\perp$ holds

$$b(\mathbf{v},p) = l(\mathbf{v}) - c(\mathbf{u},\mathbf{u},\mathbf{v}). \tag{9}$$

2.1. The Helmholtz Decomposition

In the following, the two equations (7) and (9) will be regarded as two different momentum balance equations that are, loosely speaking, a momentum balance (7) for the divergence-free forces and a momentum balance (9) for the irrotational forces. In order to justify these terms, the reader is reminded that irrotational and divergence-free vector fields are orthogonal to each other with respect to the L^2 scalar product, assuming appropriate boundary conditions and an appropriate regularity. This is true, since for an irrotational force field $\nabla\psi$ and a divergence-free flow field $\mathbf{w}$ with $\nabla\cdot\mathbf{w} = 0$ and $\mathbf{w}\cdot\mathbf{n} = 0$ for all $\mathbf{x}\in\partial\Omega$ holds

$$\begin{aligned} \int_\Omega \nabla\psi\cdot\mathbf{w}\, dx &= \int_\Omega \nabla\cdot(\psi\mathbf{w})\, dx - \int_\Omega \psi\nabla\cdot\mathbf{w}\, dx \\ &= \int_{\partial\Omega} \psi\,\mathbf{w}\cdot\mathbf{n}\, dS \\ &= 0. \end{aligned} \tag{10}$$

Moreover, according to the Helmholtz decomposition [30] every vector field $\mathbf{f} \in L^2(\Omega)^d$ can be decomposed into a divergence-free part $\mathbf{w}$, with $\nabla \cdot \mathbf{w} = 0$ and an irrotational part $\nabla\psi$, such that $\mathbf{f} = \nabla\psi + \mathbf{w}$ holds. Besides that, $\mathbf{w}$ and $\nabla\psi$ are orthogonal to each other in the L^2 scalar product. The potential ψ of the irrotational part $\nabla\psi$ can be determined uniquely by solving: search for $\psi \in H^1(\Omega)$ such that

$$\begin{aligned} \int_\Omega \nabla\psi \cdot \nabla\chi \, dx &= \int_\Omega \mathbf{f} \cdot \nabla\chi \, dx, \\ \int_\Omega \psi \, dx &= 0 \end{aligned} \tag{11}$$

holds for all $\chi \in H^1(\Omega)$, i.e., for the potential ψ homogeneous Neumann boundary conditions are assumed. Then, the divergence-free part $\mathbf{w}$ of $\mathbf{f}$ is obtained by

$$\mathbf{w} = \mathbf{f} - \nabla\psi. \tag{12}$$

The mapping $\mathbb{P}\colon L^2(\Omega)^d \to L^2(\Omega)^d$ defined by $\mathbf{f} \to \mathbf{w}$ will be called the Helmholtz projector $\mathbb{P}$ in the following [45]. Assuming that for $\mathbf{x} \in \partial\Omega$ holds $\mathbf{f} \cdot \mathbf{n} = 0$, one obtains also $\mathbf{w} \cdot \mathbf{n} = 0$ due to $\mathbf{f} = \mathbf{w} + \nabla\psi$, and the homogeneous Neumann boundary conditions $\nabla\psi \cdot \mathbf{n} = 0$.

2.2. Divergence-free Momentum Balance

The Helmholtz projector $\mathbb{P}$ will now be applied to the 'divergence-free' momentum balance (7). Here, it holds for all $\mathbf{v} \in V$

$$\int_\Omega \nu \nabla\mathbf{u} : \nabla\mathbf{v} \, dx + \int_\Omega \left((\mathbf{u} \cdot \nabla)\, \mathbf{u} \right) \cdot \mathbf{v} \, dx = \int_\Omega \mathbf{f} \cdot \mathbf{v} \, dx. \tag{13}$$

Avoiding technical difficulties, we assume that $\mathbf{f} \in L^2(\Omega)^d$ and $\mathbf{u} \in L^\infty(\Omega)^d$ hold. Then, especially $(\mathbf{u} \cdot \nabla)\, \mathbf{u} \in L^2(\Omega)^d$ holds. Since divergence-free vector fields $\mathbf{v}$ and irrotational vector fields $\nabla\psi$ are orthogonal in the L^2 scalar product, (13) can be replaced by: search for $\mathbf{u} \in$ such that

$$\int_\Omega \nu \nabla\mathbf{u} : \nabla\mathbf{v} \, dx + \int_\Omega \mathbb{P}\left((\mathbf{u} \cdot \nabla)\, \mathbf{u} \right) \cdot \mathbf{v} \, dx = \int_\Omega \mathbb{P}(\mathbf{f}) \cdot \mathbf{v} \, dx \tag{14}$$

holds for all $\mathbf{v} \in V$.

2.3. A Fundamental Invariance Property of the Incompressible Navier-Stokes Equations

Changing $\mathbf{f} \to \mathbf{f} + \nabla\psi$ in (14) yields: for all $\mathbf{v} \in V$ holds

$$\begin{aligned} \int_\Omega \nu \nabla\mathbf{u} : \nabla\mathbf{v} \, dx + \int_\Omega \mathbb{P}\left((\mathbf{u} \cdot \nabla)\, \mathbf{u} \right) \cdot \mathbf{v} \, dx &= \int_\Omega \mathbb{P}(\mathbf{f} + \nabla\psi) \cdot \mathbf{v} \, dx \\ &= \int_\Omega \mathbb{P}(\mathbf{f}) \cdot \mathbf{v}, \end{aligned} \tag{15}$$

i.e., the solution $\mathbf{u}$ does not change assuming homogeneous Dirichlet boundary conditions, since then $\mathbb{P}(\nabla\psi) = \mathbf{0}$ holds. Moreover, refering to the 'irrotational' momentum balance (9), one obtains for all $\mathbf{v} \in V^{\perp}$

$$\begin{aligned} -\int_\Omega p\nabla\cdot\mathbf{v}\,dx &= \int_\Omega (\mathbf{f}+\nabla\psi)\cdot\mathbf{v}\,dx - \int_\Omega ((\mathbf{u}\cdot\nabla)\,\mathbf{u})\cdot\mathbf{v}\,dx \\ &= -\int_\Omega \psi\nabla\cdot\mathbf{v}\,dx + \int_\Omega \mathbf{f}\cdot\mathbf{v}\,dx - \int_\Omega ((\mathbf{u}\cdot\nabla)\,\mathbf{u})\cdot\mathbf{v}\,dx, \end{aligned} \tag{16}$$

and $\mathbf{f} \to \mathbf{f} + \nabla\psi \Rightarrow p \to p + \psi$ holds. Altogether, one concludes that changing the right side by $\mathbf{f} \to \mathbf{f} + \nabla\psi$ yields a change of the solution by $(\mathbf{u}, p) \to (\mathbf{u}, p + \psi)$, i.e., the additional irrotational forcing is balanced completely by the pressure gradient. In the special case of an irrotational forcing $\nabla\psi$, one obtains due to $\mathbf{0} = \mathbf{f} \to \mathbf{f} + \nabla\psi = \nabla\psi$ the same velocity solution as for $\mathbf{f} \equiv \mathbf{0}$, i.e., $(\mathbf{u}, p) = (\mathbf{0}, \psi)$.

2.4. Consequences for Mixed Finite Elements for the Incompressible Navier-Stokes Equations

Regarding again the classical a-priori estimate (2) for exterior mixed finite element methods for the incompressible Stokes equations, one understands that the pressure part $\frac{C_2}{\nu}h^k|p|_k$ of the error term is indeed equivalent to the fact that exterior mixed methods do not fulfill the invariance property $\mathbf{f} \to \mathbf{f} + \nabla\psi \Rightarrow (\mathbf{u}, p) \to (\mathbf{u}, p + \psi)$ in a discrete sense, since otherwise the discrete velocity could not be affected by a change of the continuous pressure.

Moreover, the lack of robustness of exterior mixed finite elements for the incompressible Navier-Stokes equations can be understood by looking at (14). In exterior mixed finite element methods it is not allowed to replace the terms

$$\int_\Omega \mathbf{f}\cdot\mathbf{v}_h\,dx$$

and

$$\int_\Omega ((\mathbf{u}_h\cdot\nabla)\,\mathbf{u}_h)\cdot\mathbf{v}_h\,dx$$

by

$$\int_\Omega \mathbb{P}(\mathbf{f})\cdot\mathbf{v}_h\,dx$$

and

$$\int_\Omega \mathbb{P}\,((\mathbf{u}_h\cdot\nabla)\,\mathbf{u}_h)\cdot\mathbf{v}_h\,dx,$$

since in exterior methods discretely divergence-free vector fields $\mathbf{v}_h$ are not divergence-free, in general. Therefore, exterior mixed methods suffer from a non-physical treatment of irrotational forces. Although in the continuous setting divergence-free and irrotational forces are balanced separately, in

exterior mixed methods this strict separation breaks down and irrotational forces excite spurious discrete velocities.

In the following, we will describe an obvious resort out of this problem, using a variational crime. Assuming it was possible to replace discretely divergence-free vector fields by divergence-free ones through some kind of velocity reconstruction $\boldsymbol{\pi}_{\mathrm{h}}^{\mathrm{RT}} \mathbf{v}_h$, one could discretize the terms above as

$$\int_\Omega \mathbf{f} \cdot \boldsymbol{\pi}_{\mathrm{h}}^{\mathrm{RT}} \mathbf{v}_h \, dx \left(= \int_\Omega \mathbb{P}(\mathbf{f}) \cdot \boldsymbol{\pi}_{\mathrm{h}}^{\mathrm{RT}} \mathbf{v}_h \, dx \right)$$

and

$$\int_\Omega \left((\mathbf{u}_h \cdot \nabla) \, \mathbf{u}_h \right) \cdot \boldsymbol{\pi}_{\mathrm{h}}^{\mathrm{RT}} \mathbf{v}_h \, dx \left(= \int_\Omega \mathbb{P} \left((\mathbf{u}_h \cdot \nabla) \, \mathbf{u}_h \right) \cdot \boldsymbol{\pi}_{\mathrm{h}}^{\mathrm{RT}} \mathbf{v}_h \, dx \right),$$

leading to a more robust discrete momentum balance. In the following, this approach is applied to the classical nonconforming Crouzeix-Raviart element [15], using the lowest-order divergence-free Raviart-Thomas element [42] as velocity reconstruction.

3. A Modified Crouzeix-Raviart Element for the Incompressible Navier-Stokes Equations

3.1. Some Notation

In the following, we will denote by $\mathcal{T}_h$, $h > 0$ a family of regular finite element triangulations. For all $T \in \mathcal{T}_h$, $\mathbf{x}_T$ will abbreviate the barycenter of the simplexes T. The set of all simplex faces, i.e., edges of triangles for $d = 2$ and faces of tetrahedra for $d = 3$, will be denoted by $\bar{\mathcal{F}}_h$, and $\mathcal{F}_h$ will denote the set of interior faces. For any $F \in \bar{\mathcal{F}}_h$, $\mathbf{x}_F$ will stand for the barycenter of the face. For every face $F \in \bar{\mathcal{F}}_h$, we prescribe a face normal vector $\mathbf{n}_F$. The orientations of these normal vectors for the interior faces $F \in \mathcal{F}_h$ are arbitrary, but fixed. The orientations of $\mathbf{n}_F$ for boundary faces $F \in \bar{\mathcal{F}}_h \setminus \mathcal{F}_h$ point outward of the domain Ω. For every simplex $T \in \bar{\mathcal{T}}_h$, $\mathcal{F}_T$ will denote the set of faces of this simplex, and correspondingly, $\mathbf{n}_{T,F}$ will denote the outer normal of the simplex $T \in \mathcal{T}_h$ at its face F. If an interior face $F \in \mathcal{F}_h$ belongs to the simplices $T_1 \in \mathcal{T}_h$ and $T_2 \in \mathcal{T}_h$ with $T_1 \neq T_2$, then $T_1|T_2 := F$ will denote the face between them. Assuming now that a piecewise polynomial function $\phi \in L^\infty(\Omega)$ is given, then for every interior face $F = T_1|T_2 \in \mathcal{F}_h$ the face jump for all $\mathbf{x} \in F$ is defined by

$$[\phi](\mathbf{x}) := \left(\lim_{\substack{\mathbf{y} \to \mathbf{x} \\ \mathbf{y} \in T_1}} \phi(\mathbf{y}) \mathbf{n}_{T_1,F} + \lim_{\substack{\mathbf{y} \to \mathbf{x} \\ \mathbf{y} \in T_2}} \phi(\mathbf{y}) \mathbf{n}_{T_2,F} \right) \cdot \mathbf{n}_F.$$

Now, the space of Crouzeix-Raviart [15] velocity trial functions is given by

$$\begin{aligned} X_h := \{\mathbf{v}_h \in L^2(\Omega)^d : \mathbf{v}_{h|T} \in P_1^d \,\text{for all}\, T \in \mathcal{T}_h, \\ [\mathbf{v}_h](\mathbf{x}_F) = \mathbf{0} \,\text{for all}\, F \in \mathcal{F}_h, \\ \mathbf{v}_h(\mathbf{x}_F) = \mathbf{0} \,\text{for all}\, F \in \bar{\mathcal{F}}_h \setminus \mathcal{F}_h\}. \end{aligned} \tag{17}$$

Remark 1. *Generally, a function $\mathbf{v}_h \in V_h$ is discontinuous at element faces $F \in \mathcal{F}_h$. Continuity is prescribed only at the face barycenters. Therefore, we have $V_h \not\subset H(div;\Omega)$ [16] and discretely divergence-free function in X_h usually do not have a divergence in L^2 and are therefore not divergence-free.*

Like in Discontinuous Galerkin methods [16], we introduce the *broken gradient* $\nabla_h : X_h \to L^2(\Omega)^{d\times d}$, the *broken divergence* $\nabla_h \cdot (\cdot) : X_h \to L^2(\Omega)$, and the *broken rotation* $\nabla_h \times (\cdot) : X_h \to L^2(\Omega)^d$ such that for all $T \in \mathcal{T}_h$ hold the relations

$$\begin{aligned} (\nabla_h \mathbf{v}_h)_{|T} &:= \nabla(\mathbf{v}_{h|T}), \\ (\nabla_h \cdot \mathbf{v}_h)_{|T} &:= \nabla \cdot (\mathbf{v}_{h|T}), \\ (\nabla_h \times \mathbf{v}_h)_{|T} &:= \nabla \times (\mathbf{v}_{h|T}). \end{aligned}$$

Using the broken gradient, the space X_h will be equipped with the norm

$$\|\mathbf{v}_h\|_{1,h} := \left(\int_\Omega \nabla_h \mathbf{v}_h : \nabla_h \mathbf{v}_h \, dx\right)^{\frac{1}{2}}. \tag{18}$$

The pressure trial functions are searched for in the space

$$Q_h := \{q_h \in L_0^2(\Omega) : q_{h|T} \in P_0 \,\text{for all}\, T \in \mathcal{T}_h\}. \tag{19}$$

Further, we introduce the space of lowest order Raviart-Thomas finite elements [42] by

$$\begin{aligned} \mathrm{RT_h} := \{\mathbf{v}_h \in L^2(\Omega)^d : \mathbf{v}_{h|T}(\mathbf{x}) = \mathbf{a}_T + \frac{b_T}{d}(\mathbf{x} - \mathbf{x}_T), \text{for all } T \in \mathcal{T}_h \text{ with} \\ \mathbf{a}_T \in \mathbb{R}^d, b_T \in \mathbb{R}, \\ [\mathbf{v}_h \cdot \mathbf{n}_F](\mathbf{x}_F) = 0 \,\text{for all}\, F \in \mathcal{F}_h, \\ \mathbf{v}_h(\mathbf{x}_F) \cdot \mathbf{n}_F = 0 \,\text{for all}\, F \in \bar{\mathcal{F}}_h \setminus \mathcal{F}_h\}. \end{aligned} \tag{20}$$

Remark 2. *For a given simplex T, and a given face $F \in \mathcal{F}_T$, the value $\left(\mathbf{a}_T + \frac{b_T}{d}(\mathbf{x} - \mathbf{x}_T)\right) \cdot \mathbf{n}_F$ is constant for all $\mathbf{x} \in F$. Since $[\mathbf{v}_h \cdot \mathbf{n}_F](\mathbf{x}_F) = 0$ holds for $\mathbf{v}_h \in \mathrm{RT_h}$, we conclude that the face jumps $[\mathbf{v}_h \cdot \mathbf{n}_F](\mathbf{x})$ vanish for all $\mathbf{x} \in F$. From the continuity of the normal components of $\mathbf{v}_h$, one concludes that $\mathrm{RT_h} \subset H(div;\Omega)$ holds [16].*

Remark 3. *It holds $\mathrm{RT_h} \not\subset V_h$, since the tangential components of functions in $\mathrm{RT_h}$ need not to be continuous at face barycenters.*

3.2. Some Interpolation and Projection Operators

The usual Crouzeix-Raviart interpolation operator $\boldsymbol{\pi}_{\mathrm{h}}^{\mathrm{CR}} : X \to X_h$ is defined by

$$(\boldsymbol{\pi}_{\mathrm{h}}^{\mathrm{CR}}\,\mathbf{v})(\mathbf{x}_F) = \begin{cases} \frac{1}{|F|}\int_F \mathbf{v}\,ds, & \text{if } F \in \mathcal{F}_h, \\ \mathbf{0}, & \text{if } F \in \bar{\mathcal{F}}_h \setminus \mathcal{F}_h. \end{cases}$$

The Raviart-Thomas interpolation operator $\boldsymbol{\pi}_{\mathrm{h}}^{\mathrm{RT}} : X \cup X_h \to \mathrm{RT}_{\mathrm{h}}$ is defined by

$$\mathbf{n}_F \cdot (\boldsymbol{\pi}_{\mathrm{h}}^{\mathrm{RT}}\,\mathbf{v})(\mathbf{x}_F) = \begin{cases} \frac{1}{|F|}\int_F \mathbf{v}\cdot\mathbf{n}_F\,ds, & \text{if } F \in \mathcal{F}_h, \\ 0, & \text{if } F \in \bar{\mathcal{F}}_h \setminus \mathcal{F}_h. \end{cases}$$

In the following the Raviart-Thomas interpolation will also be applied to matrices. Then, it has to be understood as interpolation row by row. The L^2-projection $\pi_{\mathrm{h}} : Q \to Q_h$ onto the discrete pressure space is defined for any $p \in Q$ by: for all $q_h \in Q$ holds

$$\int_\Omega q_h\,\pi_{\mathrm{h}}\,p\,dx = \int_\Omega q_h p\,dx.$$

Lemma 1 (Commutative diagram property)**.** *For all $\mathbf{v} \in X$, one obtains*

$$\begin{aligned} \nabla \cdot \boldsymbol{\pi}_{\mathrm{h}}^{\mathrm{RT}}\,\mathbf{v} &= \pi_{\mathrm{h}}\,(\nabla\cdot\mathbf{v})\,, \\ \nabla_h \cdot \boldsymbol{\pi}_{\mathrm{h}}^{\mathrm{CR}}\,\mathbf{v} &= \pi_{\mathrm{h}}\,(\nabla\cdot\mathbf{v})\,. \end{aligned}$$

Especially, divergence-free vector fields are interpolated onto discrete vector fields, whose divergence, or respectively its broken divergence, vanishes.

Proof. This follows directly from the Gauss theorem and from the definitions of the Crouzeix-Raviart and Raviart-Thomas interpolation operators. □

Lemma 2. *For all $\mathbf{v} \in X \cup X_h$ it holds*

$$\|\mathbf{v} - \boldsymbol{\pi}_{\mathrm{h}}^{\mathrm{RT}}\,\mathbf{v}\|_0 \le Ch\|\mathbf{v}\|_{1,h},$$

where C does only depend on the maximum angle in $\mathcal{T}_h$.

Proof. See [2]. □

In the following, also some classical interpolation estimates are used:

Lemma 3. *For all $\mathbf{v} \in X \cap H^2(\Omega)^d$ and for all $q \in L^2(\Omega) \cap H^1(\Omega)$ hold*

$$\begin{aligned} \|\mathbf{v} - \boldsymbol{\pi}_{\mathrm{h}}^{\mathrm{CR}}\,\mathbf{v}\|_{1,h} &\le Ch|\mathbf{v}|_2, \\ \|q - \pi_{\mathrm{h}}\,q\|_0 &\le Ch|q|_1, \end{aligned}$$

where C does only depend on the mesh regularity.

3.3. The Mixed Finite Element Scheme

Introducing the discrete bilinear forms $a_h : X_h \times X_h \to \mathbb{R}$ and $b_h : X_h \times Q_h \to \mathbb{R}$, and the discrete linear form $l_h : X_h \to \mathbb{R}$, with

$$\begin{aligned} a_h(\mathbf{u}_h, \mathbf{v}_h) &:= \nu \int_\Omega \nabla_h \mathbf{u}_h : \nabla_h \mathbf{v}_h \, dx, \\ b_h(\mathbf{u}_h, q_h) &:= \int_\Omega q_h \nabla_h \cdot \mathbf{u}_h \, dx, \\ l_h(\mathbf{v}_h) &:= \int_\Omega \mathbf{f} \cdot \boldsymbol{\pi}_{\mathrm{h}}^{\mathrm{RT}} \mathbf{v}_h, \end{aligned} \tag{21}$$

the discrete incompressible Stokes problem is given by: find $(\mathbf{u}_h, p_h) \in X_h \times Q_h$ such that the equations

$$\begin{aligned} a_h(\mathbf{u}_h, \mathbf{v}_h) + b_h(\mathbf{v}_h, p_h) &= l_h(\mathbf{v}_h), \\ b_h(\mathbf{u}_h, q_h) &= 0 \end{aligned} \tag{22}$$

hold for all $(\mathbf{v}_h, q_h) \in X_h \times Q_h$.

Remark 4. *The difference of the modified scheme* (22) *w.r.t. to the classical discretization of the problem [15] concerns only the discretization of the right hand side. By committing a variational crime, discretely divergence-free vector fields* $\mathbf{v}_h$ *are mapped to divergence-free vector fields. In the case of the incompressible Navier-Stokes equations, or the incompressible Stokes equations with Coriolis force, also the left hand side has to be modified. As an example, the discretization of the incompressible Navier-Stokes equations in rotational form is presented in the numerical section of this contribution.*

Like the continuous incompressible Stokes equations, also the discretization (22) can equivalently be formulated as an elliptic problem [46, 30]. Therefore, the space of discretely divergence-free functions is introduced

$$V_h := \{\mathbf{v}_h \in X_h : b_h(\mathbf{v}_h, q_h) = 0 \text{ for all } q_h \in Q_h\}. \tag{23}$$

The discrete elliptic problem reads: search for $\mathbf{u}_h \in V_h$ such that the equations

$$a_h(\mathbf{u}_h, \mathbf{v}_h) = l_h(\mathbf{v}_h) \tag{24}$$

hold for all $\mathbf{v}_h \in V_h$.

Lemma 4.

- *For all* $h > 0$ *and all* $\mathbf{v}_h \in X_h$ *holds*

$$a_h(\mathbf{v}_h, \mathbf{v}_h) \geq \nu \|\mathbf{v}_h\|_{1,h}^2.$$

- *There is a* $\tilde{\beta} > 0$ *not depending on* h *such that for all* $h > 0$ *holds*

$$\inf_{q_h \in Q_h \setminus \{0\}} \sup_{\mathbf{v}_h \in X_h \setminus \{\mathbf{0}\}} \frac{b_h(\mathbf{v}_h, q_h)}{\|\mathbf{v}_h\|_{1,h} \|q_h\|_0} \geq \tilde{\beta}.$$

Proof. The first statement follows directly from the definitions. For the proof of the second statement, see [3]. □

4. Error Estimates

In this section, a-priori finite element error estimates for the modified Crouzeix-Raviart discretization of the incompressible Stokes equations (22) are presented. The analysis is based on the elegant estimates of the consistency error in [2] that apply the Raviart-Thomas interpolation to the best advantage and avoid the use of a trace inequality. But due to the velocity reconstruction, the new estimate for the velocity error is completely independent of the continuous pressure. First, a technical lemma is proven that actually delivers the most difficult part of the estimates.

Lemma 5. *For all* $\mathbf{v} \in X \cap H^2(\Omega)$ *and for all* $\mathbf{w} \in X + X_h$ *it holds*

$$\left| \int_\Omega \left\{ \nabla_h \mathbf{v} : \nabla_h \mathbf{w} + \Delta \mathbf{v} \cdot \boldsymbol{\pi}_{\mathrm{h}}^{\mathrm{div}} \mathbf{w} \right\} dx \right| \leq Ch \, |\mathbf{v}|_2 \, \|\mathbf{w}\|_{1,h}. \tag{25}$$

Proof. First, $\Delta \mathbf{v} \cdot \mathbf{w}$ is added to the left hand side and one obtains by the triangle inequality

$$\left| \int_\Omega \left\{ \nabla_h \mathbf{v} : \nabla_h \mathbf{w} + \Delta \mathbf{v} \cdot \boldsymbol{\pi}_{\mathrm{h}}^{\mathrm{div}} \mathbf{w} \right\} dx \right| \leq A + B,$$

with

$$A := \left| \int_\Omega \left\{ \nabla_h \mathbf{v} : \nabla_h \mathbf{w} + \Delta \mathbf{v} \cdot \mathbf{w} \right\} dx \right|,$$
$$B := \left| \int_\Omega \left\{ \Delta \mathbf{v} \cdot \left(\boldsymbol{\pi}_{\mathrm{h}}^{\mathrm{div}} \mathbf{w} - \mathbf{w} \right) \right\} dx \right|.$$

For the second term B, one directly obtains

$$B \leq \|\Delta \mathbf{v}\|_0 \, \|\boldsymbol{\pi}_{\mathrm{h}}^{\mathrm{div}} \mathbf{w} - \mathbf{w}\|_0,$$

which can be estimated as

$$B \leq Ch \, |\mathbf{v}|_2 \, \|\mathbf{w}\|_{1,h}.$$

For the first term one obtains

$$A = \left| \sum_{T \in \mathcal{T}_h} \int_{\partial T} (\nabla \mathbf{v} \cdot \mathbf{n}) \cdot \mathbf{w} \, ds \right|.$$

Following [2], one observes that $\left(\boldsymbol{\Pi}_{\mathrm{h}}^{\mathrm{RT}} \nabla \mathbf{v} \right) \cdot \mathbf{n}$ is constant on each face and continuous across the interelement boundaries. Therefore, it is easy to see that

$$\sum_{T \in \mathcal{T}_h} \int_{\partial T} \left(\left(\boldsymbol{\Pi}_{\mathrm{h}}^{\mathrm{RT}} \nabla \mathbf{v} \right) \cdot \mathbf{n} \right) \cdot \mathbf{w} \, ds = 0$$

holds for all $\mathbf{w} \in X + X_h$. Subtracting this term, we get

$$\begin{aligned} A &= \left| \sum_{T \in \mathcal{T}_h} \int_{\partial T} \left(\left(\nabla \mathbf{v} - \mathbf{\Pi}_{\mathrm{h}}^{\mathrm{RT}} \nabla \mathbf{v} \right) \cdot \mathbf{n} \right) \cdot \mathbf{w} \, ds \right| \\ &= \left| \sum_{T \in \mathcal{T}_h} \int_{T} \nabla \cdot \left(\left(\nabla \mathbf{v} - \mathbf{\Pi}_{\mathrm{h}}^{\mathrm{RT}} \nabla \mathbf{v} \right) \cdot \mathbf{w} \right) dx \right| \\ &= \left| \sum_{T \in \mathcal{T}_h} \left(\int_{T} \left(\nabla \cdot \left(\nabla \mathbf{v} - \mathbf{\Pi}_{\mathrm{h}}^{\mathrm{RT}} \nabla \mathbf{v} \right) \right) \cdot \mathbf{w} + \left(\nabla \mathbf{v} - \mathbf{\Pi}_{\mathrm{h}}^{\mathrm{RT}} \nabla \mathbf{v} \right) : \nabla \mathbf{w} \right) dx \right| \\ &\leq A_1 + A_2, \end{aligned}$$

with

$$\begin{aligned} A_1 &:= \left| \sum_{T \in \mathcal{T}_h} \int_{T} \left(\nabla \cdot \left(\nabla \mathbf{v} - \mathbf{\Pi}_{\mathrm{h}}^{\mathrm{RT}} \nabla \mathbf{v} \right) \right) \cdot \mathbf{w} \, dx \right|, \\ A_2 &:= \left| \sum_{T \in \mathcal{T}_h} \int_{T} \left(\nabla \mathbf{v} - \mathbf{\Pi}_{\mathrm{h}}^{\mathrm{RT}} \nabla \mathbf{v} \right) : \nabla \mathbf{w} \, dx \right|. \end{aligned}$$

For the second term, one obtains by classical interpolation estimates

$$|A_2| \leq Ch \, |\mathbf{v}|_2 \, \|\mathbf{w}\|_{1,h}.$$

For the first term, the commutative diagram property from Lemma 1 is applied

$$\nabla \cdot \mathbf{\Pi}_{\mathrm{h}}^{\mathrm{RT}}(\nabla \mathbf{v}) = \Pi_{\mathrm{h}} \left(\nabla \cdot (\nabla \mathbf{v}) \right) = \Pi_{\mathrm{h}} \left(\Delta \mathbf{v} \right),$$

and one obtains

$$\begin{aligned} A_1 &= \left| \sum_{T \in \mathcal{T}_h} \int_{T} \left(\nabla \cdot \left(\nabla \mathbf{v} - \mathbf{\Pi}_{\mathrm{h}}^{\mathrm{RT}} \nabla \mathbf{v} \right) \right) \cdot \mathbf{w} \, dx \right| \\ &= \left| \sum_{T \in \mathcal{T}_h} \int_{T} \left(\Delta \mathbf{v} - \Pi_{\mathrm{h}}(\Delta \mathbf{v}) \right) \cdot \mathbf{w} \, dx \right| \\ &= \left| \sum_{T \in \mathcal{T}_h} \int_{T} \Delta \mathbf{v} \cdot \left(\mathbf{w} - \Pi_{\mathrm{h}} \, \mathbf{w} \right) dx \right| \\ &\leq Ch \, |\mathbf{v}|_2 \, \|\mathbf{w}\|_{1,h}. \end{aligned}$$

□

Now, the estimate of the consistency error is a corollary to Lemma 5.

Lemma 6. *Assuming that for the solution of the continuous Stokes equations* (4) *holds* $(\mathbf{u}, p) \in H^2(\Omega)^d \times H^1(\Omega)$*. Then, the following estimate of the consistency error*

$$\frac{1}{\nu} \sup_{\mathbf{w} \in V + V_h} \frac{|a_h(\mathbf{u}, \mathbf{w}) - l_h(\mathbf{w})|}{\|\mathbf{w}\|_{1,h}} \leq Ch|\mathbf{u}|_2$$

holds.

Proof. Computing for all $\mathbf{0} \neq \mathbf{w} \in V + V_h$, one obtains

$$\begin{aligned}
\frac{1}{\nu} |a_h(\mathbf{u}, \mathbf{w}) - l_h(\mathbf{w})| &= \frac{1}{\nu} \left| \int_\Omega \left\{ \nu \nabla_h \mathbf{u} : \nabla_h \mathbf{w} - \mathbf{f} \cdot \boldsymbol{\pi}_{\mathrm{h}}^{\mathrm{div}} \mathbf{w} \right\} dx \right| \\
&= \frac{1}{\nu} \left| \int_\Omega \left\{ \nu \nabla_h \mathbf{u} : \nabla_h \mathbf{w} + (\nu \Delta \mathbf{u} - \nabla p) \cdot \boldsymbol{\pi}_{\mathrm{h}}^{\mathrm{div}} \mathbf{w} \right\} dx \right| \\
&= \left| \int_\Omega \left\{ \nabla_h \mathbf{u} : \nabla_h \mathbf{w} + \Delta \mathbf{u} \cdot \boldsymbol{\pi}_{\mathrm{h}}^{\mathrm{div}} \mathbf{w} \right\} dx \right|,
\end{aligned}$$

since the irrotational vector field ∇p is orthogonal in L^2 to the divergence-free vector field $\boldsymbol{\pi}_{\mathrm{h}}^{\mathrm{div}} \mathbf{w}$. Now, Lemma 5 delivers the desired result. □

From this estimate of the consistency error, one easily concludes the main theorem of this contribution.

Theorem 1. *Assuming that for the solution of the continuous Stokes equations* (4) *holds* $(\mathbf{u}, p) \in H^2(\Omega)^d \times H^1(\Omega)$*. Then, one obtains for the discrete solution* $(\mathbf{u}_h, p_h)$ *of the scheme* (22) *the error estimates*

$$\begin{aligned}
\|\mathbf{u} - \mathbf{u}_h\|_{1,h} &\leq Ch \, |\mathbf{u}|_2 \,, \\
\|p - p_h\|_0 &\leq C \, h \, (\nu \, |\mathbf{u}|_2 + |p|_1) \,.
\end{aligned} \tag{26}$$

Proof. i) The analysis is started from from (24), where the discrete problem is formulated as an elliptic problem in the space of discretely divergence-free functions V_h. One sets $\mathbf{w}_h := \mathbf{u}_h - \mathbf{v}_h$ for an arbitrary $\mathbf{v}_h \in V_h$. Then, one computes

$$\begin{aligned}
\nu \|\mathbf{w}_h\|_{1,h}^2 &= a_h(\mathbf{w}_h, \mathbf{w}_h) \\
&= a_h(\mathbf{u}_h - \mathbf{v}_h, \mathbf{w}_h) \\
&= a_h(\mathbf{u} - \mathbf{v}_h, \mathbf{w}_h) + a_h(\mathbf{u}_h, \mathbf{w}_h) - a_h(\mathbf{u}, \mathbf{w}_h) \\
&= a_h(\mathbf{u} - \mathbf{v}_h, \mathbf{w}_h) + l_h(\mathbf{w}_h) - a_h(\mathbf{u}, \mathbf{w}_h) \\
&\leq \nu \|\mathbf{u} - \mathbf{v}_h\|_{1,h} \|\mathbf{w}_h\|_{1,h} + |a_h(\mathbf{u}, \mathbf{w}_h) - l_h(\mathbf{w}_h)| \,.
\end{aligned}$$

Using the triangle inequality for $\|\mathbf{u} - \mathbf{u}_h\|_{1,h} = \|(\mathbf{u} - \mathbf{v}_h) - \mathbf{w}_h\|_{1,h}$, one obtains Strang's second lemma in the form

$$\|\mathbf{u} - \mathbf{u}_h\|_{1,h} \leq 2 \inf_{\mathbf{v}_h \in V_h} \|\mathbf{u} - \mathbf{v}_h\|_{1,h} + \frac{1}{\nu} \sup_{\mathbf{w}_h \in V_h} \frac{|a_h(\mathbf{u}, \mathbf{w}_h) - l_h(\mathbf{w}_h)|}{\|\mathbf{w}_h\|_{1,h}}.$$

The first error term can be bounded in a classical way, noting that

$$\inf_{\mathbf{v}_h \in V_h} \|\mathbf{u} - \mathbf{v}_h\|_{1,h} \leq \|\mathbf{u} - \boldsymbol{\pi}_{\mathrm{h}}^{\mathrm{CR}} \mathbf{u}\|_{1,h}$$

holds due to Lemma 1. Therefore, classical interpolation theory [15] delivers

$$\|\mathbf{u} - \boldsymbol{\pi}_{\mathrm{h}}^{\mathrm{CR}} \mathbf{u}\|_{1,h} \leq Ch|\mathbf{u}|_2.$$

Together with Lemma 6 the first error estimate is proven.

ii) For the pressure estimate it is noted first that

$$\|p - p_h\|_0 \leq \|p - \pi_{\mathrm{h}} p\|_0 + \|\pi_{\mathrm{h}} p - p_h\|_0$$

holds. Obviously, the first term is bounded by

$$\|p - p_h\|_0 \leq Ch\,|p|_1\,.$$

Due to the discrete inf-sup stability from Lemma 4 the second term can be estimated by

$$\|\pi_{\mathrm{h}} p - p_h\|_0 \leq \frac{1}{\tilde{\beta}} \sup_{\mathbf{v}_h \in V_h} \frac{b_h(\mathbf{v}_h, \pi_{\mathrm{h}} p - p_h)}{\|\mathbf{v}_h\|_{1,h}}.$$

The term in the denominator of this expression can be split into two parts by

$$b_h(\mathbf{v}_h, \pi_{\mathrm{h}} p - p_h) = b_h(\mathbf{v}_h, \pi_{\mathrm{h}} p - p) + b_h(\mathbf{v}_h, p - p_h).$$

The first term can be estimated by

$$|b_h(\mathbf{v}_h, \pi_{\mathrm{h}} p - p)| \leq \sqrt{d}\,\|\mathbf{v}_h\|_{1,h} \|p - \pi_{\mathrm{h}} p\|_0 \leq Ch\,|p|_1 \cdot \|\mathbf{v}_h\|_{1,h}.$$

For the second term one computes

$$\begin{aligned}
b_h(\mathbf{v}_h, p - p_h) &= b_h(\mathbf{v}_h, p) + a_h(\mathbf{u}_h, \mathbf{v}_h) - l_h(\mathbf{v}_h) \\
&= a_h(\mathbf{u}_h - \mathbf{u}, \mathbf{v}_h) \\
&\quad + \int_\Omega \left\{ \nu \nabla_h \mathbf{u} : \nabla_h \mathbf{v}_h - p \nabla_h \cdot \mathbf{v}_h - \mathbf{f} \cdot \boldsymbol{\pi}_{\mathrm{h}}^{\mathrm{div}} \mathbf{v}_h \right\} dx \\
&= a_h(\mathbf{u}_h - \mathbf{u}, \mathbf{v}_h) \\
&\quad + \int_\Omega \nu \left\{ \nabla_h \mathbf{u} : \nabla_h \mathbf{v}_h + \Delta \mathbf{u} \cdot \boldsymbol{\pi}_{\mathrm{h}}^{\mathrm{div}} \mathbf{v}_h \right\} dx,
\end{aligned}$$

since

$$\begin{aligned}
\int_\Omega \left\{ -p \nabla_h \cdot \mathbf{v}_h - \nabla p \cdot \left(\boldsymbol{\pi}_{\mathrm{h}}^{\mathrm{div}} \mathbf{v}_h \right) \right\} dx &= \int_\Omega \left\{ -p \nabla_h \cdot \mathbf{v}_h + p \nabla \cdot \left(\boldsymbol{\pi}_{\mathrm{h}}^{\mathrm{div}} \mathbf{v}_h \right) \right\} dx \\
&= \int_\Omega \left\{ -p \nabla_h \cdot \mathbf{v}_h + p \nabla_h \cdot \mathbf{v}_h \right\} dx \\
&= 0
\end{aligned}$$

holds. Therefore, one obtains the estimate

$$b_h(\mathbf{v}_h, p - p_h) \leq C\nu h \left|\mathbf{u}\right|_2 \left\|\mathbf{v}_h\right\|_{1,h},$$

and one finally has the pressure error estimate

$$\left\|p - p_h\right\|_0 \leq C \left\{ \frac{1}{\tilde{\beta}} \nu \left|\mathbf{u}\right|_2 + \left(1 + \frac{1}{\tilde{\beta}}\right) \left|p\right|_1 \right\} h.$$

□

Remark 5. *The considerations above deliver optimal a-priori error estimates for the discrete gradient norm of the velocity and the L^2 norm of the pressure. Numerically, it can be seen in the next section that also the L^2 norm of the velocity seems to converge with optimal order on unstructured triangle meshes. Unfortunately, proving an optimal error estimate for the L^2 norm of the velocity by duality techniques needs superconvergence properties of the Raviart-Thomas interpolation operator due to the velocity reconstruction with piecewise lowest-order Raviart-Thomas vector fields. This leads to very restrictive mesh assumptions as investigated in [6], and seems to be unavoidable in theory. In a personal communication, Joachim Schöberl from the Vienna University of Technology advised the author to employ first order Brezzi-Douglas-Marini elements for the velocity reconstruction. Then, an optimal a-priori L^2 error estimate for the velocity can be proven, but the velocity reconstruction becomes more complicated.*

5. Numerical Results

In the following, several examples are presented that illustrate the theoretical findings above. First, we start with some academic test problems comparing the convergence behaviour of the classical Crouzeix-Raviart element with the modified scheme.

5.1. The Best Case for the Classical Crouzeix-Raviart Element

The first example is a linear Stokes problem with kinematic viscosity $\nu = 1$ in the domain $\Omega = [0,1]^2$. The velocity field is derived from the stream function $\xi = x^2(1-x)^2y^2(1-y)^2$ delivering a polynomial $\mathbf{u} = \operatorname{rot}\xi$ of seventh order as velocity solution, see Fig. 2, left picture. This velocity solution has homogeneous Dirichlet boundary conditions and lies in $H_0^1(\Omega)^2$. Due to the introduction of the velocity reconstruction into the discrete variational formulation, one may guess that this additional consistency error will decrease the accuracy of the new modified Crouzeix-Raviart scheme compared to the classical one. In order to quantify this reduction of accuracy, we prescribe $p = 0$ as the pressure solution and compute the right hand side by

$$\mathbf{f} = -\nu\Delta\mathbf{u} + \nabla p.$$

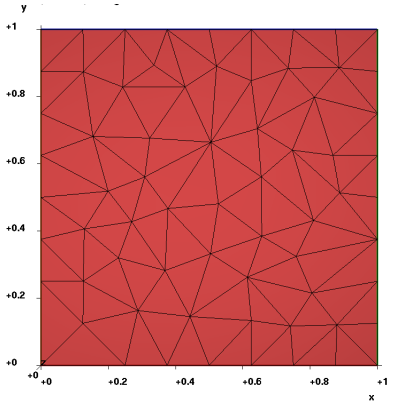

Figure 1: Coarse grid Delaunay mesh for the numerical computations

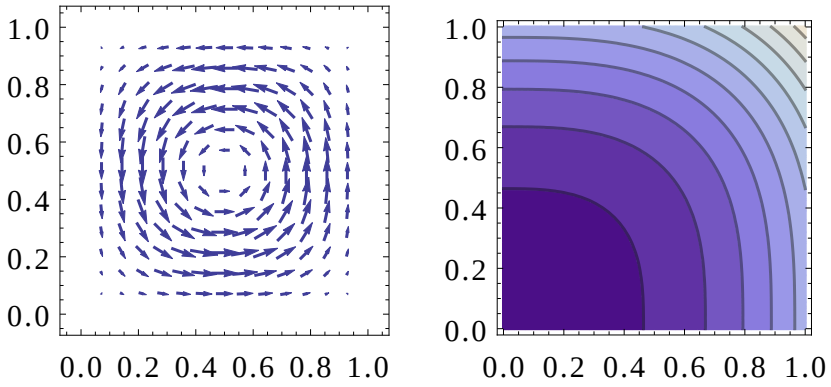

Figure 2: Left: velocity field $\mathbf{u} = \text{rot}\,\left(x^2(1-x)^2y^2(1-y)^2\right)$, right: pressure $p = x^3+y^3-\frac{1}{2}$

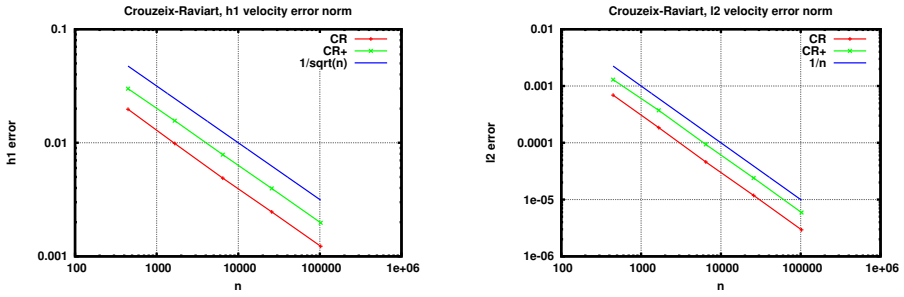

Figure 3: Problem 1: Comparison of the classical Crouzeix-Raviart element (red), and the modified Crouzeix-Raviart scheme with velocity reconstruction (green). Left: discrete H^1 velocity error norms, right: L^2 velocity error norms. n denotes the number of degrees of freedom

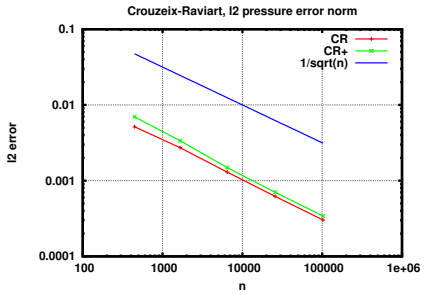

Figure 4: Problem 1: Comparison of the classical Crouzeix-Raviart element (red), and the modified Crouzeix-Raviart scheme with velocity reconstruction (green). Plotted: L^2 pressure error norms. n denotes the number of degrees of freedom

ndofs	$\|\mathbf{u} - \mathbf{u}_h\|_{1,h}$	$\|\mathbf{u} - \mathbf{u}_h\|_0$	$\|p - p_h\|_0$
446	$1.9723240 \cdot 10^{-2}$	$6.8893961 \cdot 10^{-4}$	$5.1439364 \cdot 10^{-3}$
1,665	$9.8618544 \cdot 10^{-3}$	$1.8502989 \cdot 10^{-4}$	$2.7202521 \cdot 10^{-3}$
6,466	$4.8831874 \cdot 10^{-3}$	$4.5949125 \cdot 10^{-5}$	$1.2962826 \cdot 10^{-3}$
25,700	$2.4647824 \cdot 10^{-3}$	$1.1822667 \cdot 10^{-5}$	$6.2107982 \cdot 10^{-4}$
102,414	$1.2277389 \cdot 10^{-3}$	$2.9328399 \cdot 10^{-6}$	$3.0273344 \cdot 10^{-4}$

Table 1: Problem 1: Numerical results for the classical Crouzeix-Raviart element

Since the continuous pressure p vanishes in Ω, the pressure part $\frac{C_2}{\nu} h|p|_1$ of the error estimate (2) for the classical Crouzeix-Raviart element vanishes as well, and we will obtain the best discrete velocity solution that the classical Crouzeix-Raviart element is able to deliver. We compare the two schemes on a sequence of unstructured isotropic Delaunay meshes that are constructed by the mesh generator TRIANGLE [44], see Fig. 1 for a picture of the coarsest grid used in the numerical experiments. A comparison of the numerical results is given in Fig. 3 and Fig. 4. Here, the discrete H^1 error norms and the L^2 error norms are plotted against the number of degrees of freedom n. Note that for 2D problems holds $\frac{1}{\sqrt{n}} \sim h$, with h being the mesh size of the grid. One can recognize that both methods seem to converge with asymptotically optimal experimental orders of convergence in all three norms. From the exact values of the numerical results in Tables 1 and 2 it is affirmed that indeed the classical method performs better for this example. The velocity error norms of the classical method are about two times smaller than the error norms of the modified scheme. The pressure error norms seem to become closer and closer, as the mesh size decreases.

5.2. The Dependence on the Pressure

In the second numerical example, it will be demonstrated that the new modified scheme is much more robust with respect to irrotational forces

ndofs	$\|\mathbf{u}-\mathbf{u}_h\|_{1,h}$	$\|\mathbf{u}-\mathbf{u}_h\|_0$	$\|p-p_h\|_0$
446	$2.9946608 \cdot 10^{-2}$	$1.2931374 \cdot 10^{-3}$	$6.9603779 \cdot 10^{-3}$
1,665	$1.5652884 \cdot 10^{-2}$	$3.7250738 \cdot 10^{-4}$	$3.3688954 \cdot 10^{-3}$
6,466	$7.8571074 \cdot 10^{-3}$	$9.3562095 \cdot 10^{-5}$	$1.4855866 \cdot 10^{-3}$
25,700	$3.9649366 \cdot 10^{-3}$	$2.3990350 \cdot 10^{-5}$	$7.0393677 \cdot 10^{-4}$
102,414	$1.9755105 \cdot 10^{-3}$	$5.9092147 \cdot 10^{-6}$	$3.4122439 \cdot 10^{-4}$

Table 2: Problem 1: Numerical results for the modified Crouzeix-Raviart element

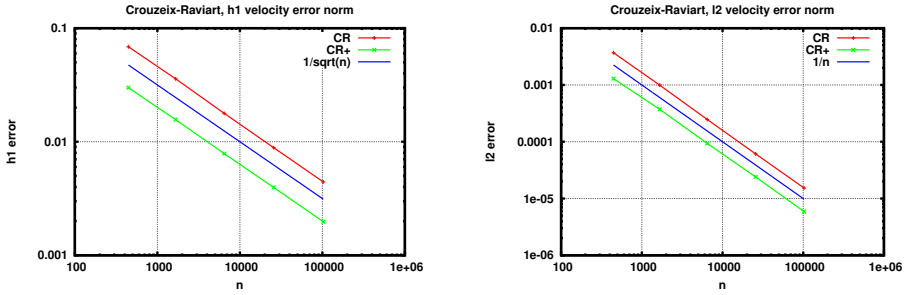

Figure 5: Problem 2, $\nu = 1$: Comparison of the classical Crouzeix-Raviart element (red), and the modified Crouzeix-Raviart scheme with velocity reconstruction (green). Left: discrete H^1 velocity error norms, right: L^2 velocity error norms. n denotes the number of degrees of freedom

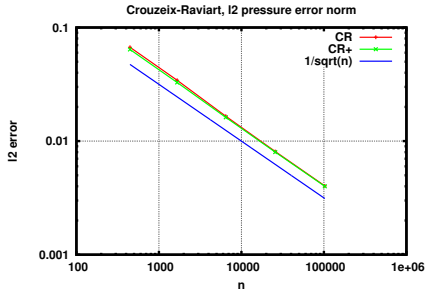

Figure 6: Problem 2, $\nu = 1$: Comparison of the classical Crouzeix-Raviart element (red), and the modified Crouzeix-Raviart scheme with velocity reconstruction (green). Plotted: L^2 pressure error norms. n denotes the number of degrees of freedom

in the right side of the incompressible Stokes equations. In order to show this, we modify the first example only slightly by prescribing an academic pressure solution $p = x^3 + y^3 - \frac{1}{2}$, see Fig. 2, right picture. By prescribing $\nu = 1$ and $\nu = 10^{-3}$, two different numerical experiments are performed. For $\nu = 1$, the comparison of the numerical results for the classical Crouzeix-Raviart element and the modified scheme can be found in Fig. 5, Fig. 6,

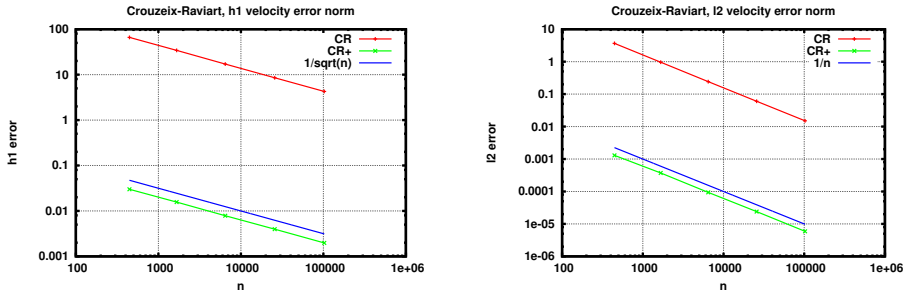

Figure 7: Problem 2, $\nu = 10^{-3}$: Comparison of the classical Crouzeix-Raviart element (red), and the modified Crouzeix-Raviart scheme with velocity reconstruction (green). Left: discrete H^1 velocity error norms, right: L^2 velocity error norms. n denotes the number of degrees of freedom

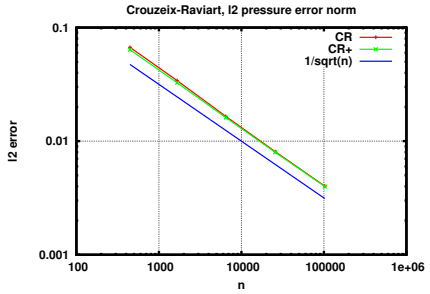

Figure 8: Problem 2, $\nu = 10^{-3}$: Comparison of the classical Crouzeix-Raviart element (red), and the modified Crouzeix-Raviart scheme with velocity reconstruction (green). Plotted: L^2 pressure error norms. n denotes the number of degrees of freedom

Tab. 3, and Tab. 4. It can be observed from the numerical experiments that the classical Crouzeix-Raviart element is indeed not robust against changes in the continuous pressure that has to be approximated. This illustrates that the classical Crouzeix-Raviart elements violates the fundamental invariance $\mathbf{f} \to \mathbf{f} + \nabla\psi \Rightarrow (\mathbf{u}, p) \to (\mathbf{u}, p + \psi)$ of the continuous incompressible Stokes equations. On the other hand, the modified Crouzeix-Raviart is robust against irrotational forces in the momentum equations and delivers a pressure-independent discrete velocity solution. It is surprising that the modified scheme delivers even for $\nu = 1$ a slightly better velocity approximation than the classical scheme. Therefore, the reduced consistency of the modified scheme due to the velocity reconstruction is compensated by the fact that it has no pressure term in its a-priori error estimate for the discrete velocity (see Theorem 1), contrary to the classical estimate (2). Moreover, for $\nu = 10^{-3}$ the modified scheme is dramatically superior to the classical one, see Fig. 7, Fig. 8, Tab. 5, and Fig. 6. Obviously, this gain of accu-

ndofs	$\|\mathbf{u}-\mathbf{u}_h\|_{1,h}$	$\|\mathbf{u}-\mathbf{u}_h\|_0$	$\|p-p_h\|_0$
446	$6.8484997 \cdot 10^{-2}$	$3.6952646 \cdot 10^{-3}$	$6.7005149 \cdot 10^{-2}$
1,665	$3.5804448 \cdot 10^{-2}$	$9.9304981 \cdot 10^{-4}$	$3.4325277 \cdot 10^{-2}$
6,466	$1.7765810 \cdot 10^{-2}$	$2.4660675 \cdot 10^{-4}$	$1.6574087 \cdot 10^{-2}$
25,700	$8.8641022 \cdot 10^{-3}$	$6.1130411 \cdot 10^{-5}$	$8.1046570 \cdot 10^{-3}$
102,414	$4.4328035 \cdot 10^{-3}$	$1.5315213 \cdot 10^{-5}$	$4.0349564 \cdot 10^{-3}$

Table 3: Problem 2, $\nu = 1$: Numerical results for the classical Crouzeix-Raviart element

ndofs	$\|\mathbf{u}-\mathbf{u}_h\|_{1,h}$	$\|\mathbf{u}-\mathbf{u}_h\|_0$	$\|p-p_h\|_0$
446	$2.9946608 \cdot 10^{-2}$	$1.2931374 \cdot 10^{-3}$	$6.4124852 \cdot 10^{-2}$
1,665	$1.5652884 \cdot 10^{-2}$	$3.7250738 \cdot 10^{-4}$	$3.2820564 \cdot 10^{-2}$
6,466	$7.8571074 \cdot 10^{-3}$	$9.3562095 \cdot 10^{-5}$	$1.6195238 \cdot 10^{-2}$
25,700	$3.9649366 \cdot 10^{-3}$	$2.3990350 \cdot 10^{-5}$	$8.0054984 \cdot 10^{-3}$
102,414	$1.9755105 \cdot 10^{-3}$	$5.9092147 \cdot 10^{-6}$	$3.9995703 \cdot 10^{-4}$

Table 4: Problem 2, $\nu = 1$: Numerical results for the modified Crouzeix-Raviart element

racy can be made arbitarily large by using smaller and smaller kinematic viscosities ν.

5.3. Hagen-Poiseuille Flow

In the third numerical example, a nonlinear Navier-Stokes problem will be investigated. We will study a case, where the right hand side of the momentum equations is zero, i.e., $\mathbf{f} \equiv \mathbf{0}$. Therefore, the flow is completely driven by boundary conditions. The example serves to illustrate the significance of a correct treatment of irrotational forces in the *left hand side* of the momentum equations. As a guiding example, we will investigate the incompressible Navier-Stokes equations in *rotational form* [34], i.e., we

ndofs	$\|\mathbf{u}-\mathbf{u}_h\|_{1,h}$	$\|\mathbf{u}-\mathbf{u}_h\|_0$	$\|p-p_h\|_0$
446	$6.6020271 \cdot 10^{1}$	$3.6549659 \cdot 10^{0}$	$6.6934810 \cdot 10^{-2}$
1,665	$3.4249307 \cdot 10^{1}$	$9.5981712 \cdot 10^{-1}$	$3.4142423 \cdot 10^{-2}$
6,466	$1.7113970 \cdot 10^{1}$	$2.4181699 \cdot 10^{-1}$	$1.6525201 \cdot 10^{-2}$
25,700	$8.5255475 \cdot 10^{0}$	$6.0181574 \cdot 10^{-2}$	$8.0833147 \cdot 10^{-3}$
102,414	$4.2607646 \cdot 10^{0}$	$1.5037126 \cdot 10^{-2}$	$4.0236664 \cdot 10^{-3}$

Table 5: Problem 2, $\nu = 10^{-3}$: Numerical results for the classical Crouzeix-Raviart element

ndofs	$\|\mathbf{u}-\mathbf{u}_h\|_{1,h}$	$\|\mathbf{u}-\mathbf{u}_h\|_0$	$\|p-p_h\|_0$
446	$2.9946608 \cdot 10^{-2}$	$1.2931374 \cdot 10^{-3}$	$6.3745979 \cdot 10^{-2}$
1,665	$1.5652884 \cdot 10^{-2}$	$3.7250738 \cdot 10^{-4}$	$3.2647205 \cdot 10^{-2}$
6,466	$7.8571074 \cdot 10^{-3}$	$9.3562095 \cdot 10^{-5}$	$1.6126958 \cdot 10^{-2}$
25,700	$3.9649366 \cdot 10^{-3}$	$2.3990350 \cdot 10^{-5}$	$7.9744892 \cdot 10^{-3}$
102,414	$1.9755105 \cdot 10^{-3}$	$5.9092147 \cdot 10^{-6}$	$3.9849879 \cdot 10^{-4}$

Table 6: Problem 2, $\nu = 10^{-3}$: Numerical results for the modified Crouzeix-Raviart element

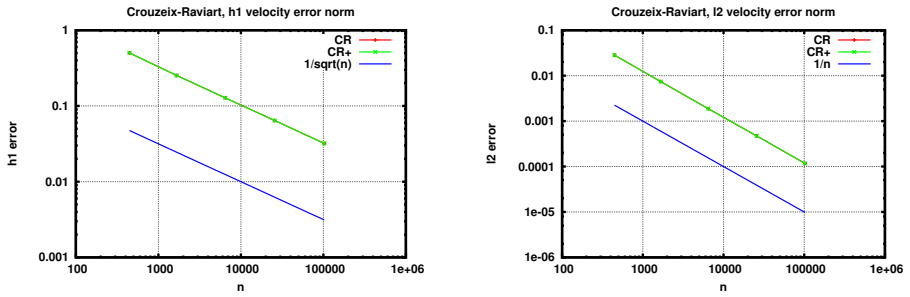

Figure 9: Problem 3 (linear), $\nu = 10^{-2}$: Comparison of the classical Crouzeix-Raviart element (red), and the modified Crouzeix-Raviart scheme with velocity reconstruction (green). Left: discrete H^1 velocity error norms, right: L^2 velocity error norms. n denotes the number of degrees of freedom

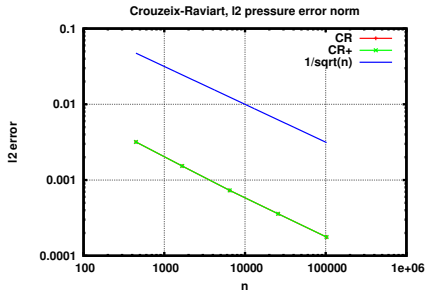

Figure 10: Problem 3 (linear): Comparison of the classical Crouzeix-Raviart element (red), and the modified Crouzeix-Raviart scheme with velocity reconstruction (green). Plotted: L^2 pressure error norms. n denotes the number of degrees of freedom

discretize

$$-\nu\Delta\mathbf{u} + (\nabla \times \mathbf{u}) \times \mathbf{u} + \nabla P = \mathbf{f},$$
$$-\nabla \cdot \mathbf{u} = 0.$$

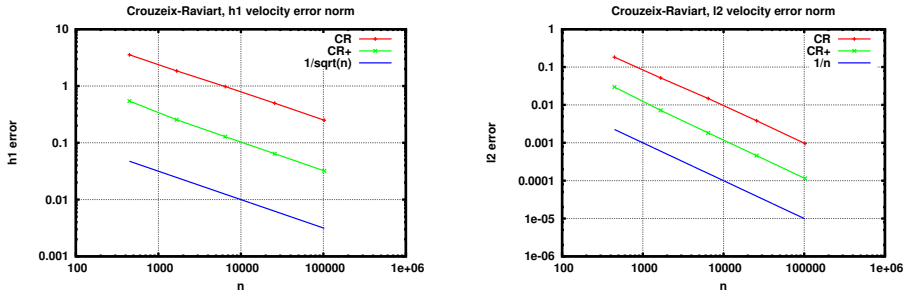

Figure 11: Problem 3 (nonlinear), $\nu = 10^{-2}$: Comparison of the classical Crouzeix-Raviart element (red), and the modified Crouzeix-Raviart scheme with velocity reconstruction (green). Left: discrete H^1 velocity error norms, right: L^2 velocity error norms. n denotes the number of degrees of freedom

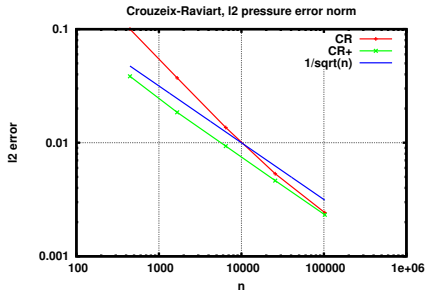

Figure 12: Problem 3 (nonlinear), $\nu = 10^{-2}$: Comparison of the classical Crouzeix-Raviart element (red), and the modified Crouzeix-Raviart scheme with velocity reconstruction (green). Plotted: L^2 pressure error norms. n denotes the number of degrees of freedom

The rotational form is one of several possibilities for the formulation of the continuous incompressible Navier-Stokes equations. It is based on the vector identity

$$(\mathbf{u} \cdot \nabla)\,\mathbf{u} \equiv (\nabla \times \mathbf{u}) \times \mathbf{u} + \frac{1}{2}\nabla\left(\mathbf{u}^2\right).$$

In the rotational form of the incompressible Navier-Stokes equations the irrotational term $\frac{1}{2}\nabla\left(\mathbf{u}^2\right)$ is absorbed into the so-called Bernoulli pressure $P = p + \frac{1}{2}\nabla\left(\mathbf{u}^2\right)$. Discretizing the incompressible Navier-Stokes equations in rotational form is not very popular in CFD, because it is known to deliver inaccurate results [34], even for very simple flow problems. On the other hand, it is also known that grad-div stabilization greatly improves robustness and accuracy of discretizations based on the rotational form. Moreover, divergence-free flow solvers deliver the same discrete velocity solution, independent of the fact, whether the rotational or the convection form of the Navier-Stokes equations is employed [4]. Therefore, we investigate the classical Hagen-Poiseuille flow in a two-dimensional channel. We investigate the

problem for a moderate kinematic viscosity $\nu = 10^{-2}$ and want to approximate the quadratic velocity field

$$\begin{pmatrix} u \\ v \end{pmatrix} = 4.0y(1-y) \begin{pmatrix} 1 \\ 0 \end{pmatrix}.$$

The kinematic pressure is given by $p = 8\nu\left(\frac{1}{2} - x\right)$. Correspondingly, the Bernoulli pressure is $P = p + \frac{1}{2}\mathbf{u}^2 - \frac{4}{15}$. In our numerical experiments on Hagen-Poiseuille flow, we always prescribe simple inhomogeneous Dirichlet boundary conditions for the velocity, i.e., we compute boundary integrals

$$\frac{1}{|F|}\int_F \mathbf{u}\, dS$$

and assign these face averages to the corresponding velocity degrees of freedom. For this problem, the nonlinear term $(\mathbf{u}\cdot\nabla)\mathbf{u}$ vanishes, i.e., it is a stable solution of the incompressible Stokes *and* the incompressible Navier-Stokes equations at the same time, as long as the kinematic viscosity ν is large enough. Now, Hagen-Poiseuille flow is an interesting numerical Benchmark for the Crouzeix-Raviart element due to two reasons. First, neither the velocity solution, nor the kinematic and the Bernoulli pressure are in the trial spaces of the Crouzeix-Raviart element. Therefore, the Crouzeix-Raviart element can only approximate this simple flow problem. Second, the nonlinear term in rotational form is interesting for this problem, since it holds $(\mathbf{u}\cdot\nabla)\mathbf{u} \equiv \mathbf{0}$. Therefore, the nonlinear term

$$(\nabla\times\mathbf{u})\times\mathbf{u} = (\mathbf{u}\cdot\nabla)\,\mathbf{u} - \frac{1}{2}\nabla\left(\mathbf{u}^2\right) = -\frac{1}{2}\nabla\left(\mathbf{u}^2\right)$$

is completely irrotational in the case of Hagen-Poisseuille flow. A numerical approximation $(\nabla_h\times\mathbf{u}_h)\times\mathbf{u}_h$ is therefore expected to have at least a large irrotational part in the sense of the Helmholtz decomposition in L^2, and a discretization using velocity reconstructions is expected to deliver more accurate results.

In order to obtain some kind of reference solution, we investigate first the behaviour of the Crouzeix-Raviart element in the case of the linear Stokes problem. The numerical results in this situation are presented in Fig. 9, Fig. 10, and Tab. 7. It is not surprising that in the linear Stokes problem, the classical Crouzeix-Raviart element and the modified scheme deliver exactly the same results. Since the left hand side for the Stokes case is identical for both schemes, only the right hand side could differ. But due to $\mathbf{f} \equiv \mathbf{0}$ both discrete right hand sides vanish and are identical, too. All three error norms seem to converge with an asyptotically optimal experimental order of convergence.

For the nonlinear problem, we discretize the nonlinear term in rotational form for the classical Crouzeix-Raviart element in the standard way as

$$\int_\Omega ((\nabla_h\times\mathbf{u}_h)\times\mathbf{u}_h)\cdot\mathbf{v}_h\, dx.$$

ndofs	$\|\mathbf{u}-\mathbf{u}_h\|_{1,h}$	$\|\mathbf{u}-\mathbf{u}_h\|_0$	$\|p-p_h\|_0$
446	$5.0124012 \cdot 10^{-1}$	$2.8307955 \cdot 10^{-2}$	$3.1851622 \cdot 10^{-3}$
1,665	$2.5310639 \cdot 10^{-1}$	$7.4014036 \cdot 10^{-3}$	$1.5315692 \cdot 10^{-3}$
6,466	$1.2789337 \cdot 10^{-1}$	$1.8743517 \cdot 10^{-3}$	$7.2983392 \cdot 10^{-4}$
25,700	$6.4169631 \cdot 10^{-2}$	$4.7225534 \cdot 10^{-4}$	$3.5844523 \cdot 10^{-4}$
102,414	$3.1992647 \cdot 10^{-2}$	$1.1693987 \cdot 10^{-4}$	$1.7674005 \cdot 10^{-4}$

Table 7: Problem 3 (linear): Numerical results for the classical and the modified Crouzeix-Raviart element

For the modified Crouzeix-Raviart scheme we use two velocity reconstructions

$$\int_\Omega \left((\nabla_h \times \mathbf{u}_h) \times \boldsymbol{\pi}_{\mathrm{h}}^{\mathrm{RT}}(\mathbf{u}_h)\right) \cdot \boldsymbol{\pi}_{\mathrm{h}}^{\mathrm{RT}}(\mathbf{v}_h) dx.$$

The velocity reconstruction of the test function $\mathbf{v}_h$ makes the discrete nonlinear term robust with respect to irrotational forces, and the velocity reconstruction of $\mathbf{u}_h$ makes the discrete nonlinear term antisymmetric.

The numerical results for the nonlinear Hagen-Poiseuille problem are presented in Fig. 11 and Fig. 12, Tab. 8, and Tab. 9. The nonlinear iteration was solved by up to 38 Picard iterations, until the nonlinear residuum measured in a discrete l_1-norm was smaller than 10^{-13}. The nonlinear iteration was started with the solution of the linear Stokes problem. Again, all the three error norms seem to have an asymptotically optimal experimental order of convergence, but the velocity error of the modified scheme is about one order smaller than the velocity error of the classical Crouzeix-Raviart element. The classical Crouzeix-Raviart element suffers from a significant loss of accuracy, when comparing the numerical results for the Stokes problem and the Navier-Stokes problem. Obviously, the (almost completely) irrotational term $(\nabla_h \times \mathbf{u}_h) \times \mathbf{u}_h$ perturbs the momentum balance in a disadvantageous manner. On the other hand, the discrete velocity for the modified scheme does not change much, when solving the nonlinear problem instead of the linear one. This is due to the sophisticated discretization of the nonlinear term in the modified scheme, where $(\nabla_h \times \mathbf{u}_h) \times \boldsymbol{\pi}_{\mathrm{h}}^{\mathrm{RT}}(\mathbf{u}_h)$ is almost irrotational in the sense of the Helmholtz decomposition in L^2. But obviously it cannot expected that this term is completely irrotational, since it is only a discrete approximation of $(\nabla \times \mathbf{u}) \times \mathbf{u}$.

Last but not least, some results are reported, if $\nu = 10^{-3}$ is chosen. Then, the nonlinear Picard iteration does converge only beginning with the fourth refinement level. Again, up to 38 Picard iteration were needed to decrease the nonlinear residuum down to 10^{-13}. The corresponding numerical results are reported in Tab. 10, and Tab. 11. This time the velocity error of the modified Crouzeix-Raviart is about 2 orders of magnitude smaller, meeting the expectation that the velocity error of the classical Crouzeix-Raviart

ndofs	$\|\mathbf{u}-\mathbf{u}_h\|_{1,h}$	$\|\mathbf{u}-\mathbf{u}_h\|_0$	$\|p-p_h\|_0$
446	$3.5464232 \cdot 10^{0}$	$1.8260081 \cdot 10^{-1}$	$9.9976663 \cdot 10^{-2}$
1,665	$1.8452666 \cdot 10^{0}$	$5.1646526 \cdot 10^{-2}$	$3.7245478 \cdot 10^{-2}$
6,466	$9.7851623 \cdot 10^{-1}$	$1.4768490 \cdot 10^{-2}$	$1.3621778 \cdot 10^{-2}$
25,700	$4.9794575 \cdot 10^{-1}$	$3.8231564 \cdot 10^{-3}$	$5.3326950 \cdot 10^{-3}$
102,414	$2.4952718 \cdot 10^{-1}$	$9.5480858 \cdot 10^{-4}$	$2.4258945 \cdot 10^{-3}$

Table 8: Problem 3 (nonlinear), $\nu = 10^{-2}$: Numerical results for the classical Crouzeix-Raviart element

ndofs	$\|\mathbf{u}-\mathbf{u}_h\|_{1,h}$	$\|\mathbf{u}-\mathbf{u}_h\|_0$	$\|p-p_h\|_0$
446	$5.4269363 \cdot 10^{-1}$	$2.9717691 \cdot 10^{-2}$	$3.8422682 \cdot 10^{-2}$
1,665	$2.5488774 \cdot 10^{-1}$	$7.1959470 \cdot 10^{-3}$	$1.8516677 \cdot 10^{-2}$
6,466	$1.2814866 \cdot 10^{-1}$	$1.8240090 \cdot 10^{-3}$	$9.3384590 \cdot 10^{-3}$
25,700	$6.4205284 \cdot 10^{-2}$	$4.5868013 \cdot 10^{-4}$	$1.1388098 \cdot 10^{-3}$
102,414	$3.2000515 \cdot 10^{-2}$	$1.1388098 \cdot 10^{-4}$	$2.3234214 \cdot 10^{-3}$

Table 9: Problem 3 (nonlinear), $\nu = 10^{-2}$: Numerical results for the modified Crouzeix-Raviart element

element should scale with $\frac{1}{\nu}$ as in the linear case.

5.4. Driven Cavity Flow

In the last example, we will again look at a flow that is completely driven by boundary conditions, i.e., where $\mathbf{f} \equiv \mathbf{0}$ holds. Such an example is the driven cavity problem in a square domain $\Omega = [0,1]^2$ with Reynolds number 100, i.e., with $\nu = 10^{-2}$. In this case, the nonlinear term in rotational form $(\nabla \times \mathbf{u}) \times \mathbf{u}$ has definitely an important divergence-free part in the sense of the Helmholtz decomposition. On the other hand, it is expected that this term also has an irrotational part that could spoil the numerical accuracy of the classical Crouzeix-Raviart element. Since there is not an exact solution available, only the convergence behaviour of a specific functional of the solution is used for measuring and comparing the quality of the two different numerical discretization schemes. As a functional the L^2 norm of the velocity field is chosen, since this value is easy to compute. The computed

ndofs	$\|\mathbf{u}-\mathbf{u}_h\|_{1,h}$	$\|\mathbf{u}-\mathbf{u}_h\|_0$	$\|p-p_h\|_0$
25,700	$4.8965197 \cdot 10^{0}$	$3.8107763 \cdot 10^{-2}$	$2.2691657 \cdot 10^{-2}$
102,414	$2.4652387 \cdot 10^{0}$	$1.0523624 \cdot 10^{-2}$	$6.6753413 \cdot 10^{-3}$

Table 10: Problem 3 (nonlinear), $\nu = 10^{-3}$: Numerical results for the classical Crouzeix-Raviart element

ndofs	$\|\mathbf{u}-\mathbf{u}_h\|_{1,h}$	$\|\mathbf{u}-\mathbf{u}_h\|_0$	$\|p-p_h\|_0$
25,700	$6.8734350 \cdot 10^{-2}$	$4.8073915 \cdot 10^{-4}$	$4.6283131 \cdot 10^{-3}$
102,414	$4.0890676 \cdot 10^{-2}$	$1.3855210 \cdot 10^{-4}$	$2.3179468 \cdot 10^{-3}$

Table 11: Problem 3 (nonlinear), $\nu = 10^{-3}$: Numerical results for the modified Crouzeix-Raviart element

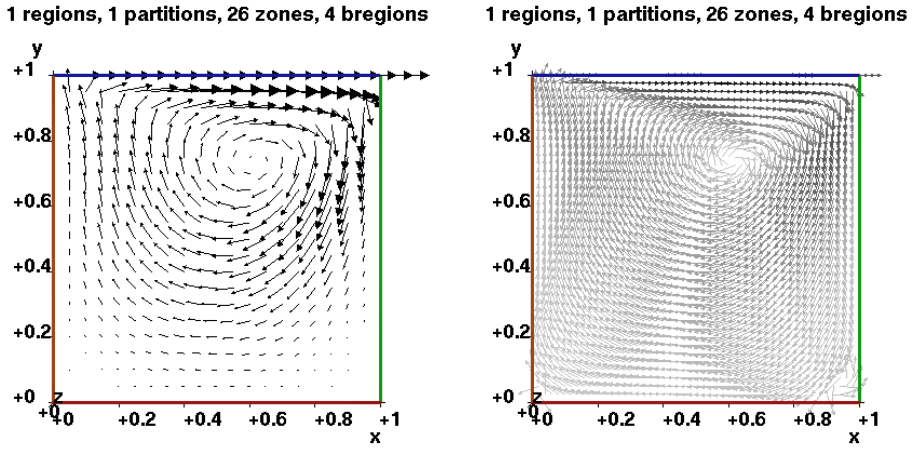

Figure 13: Problem 4 (nonlinear): Velocity field (left) and stream lines (right) of the driven cavity problem at $\mathrm{Re} = 100$

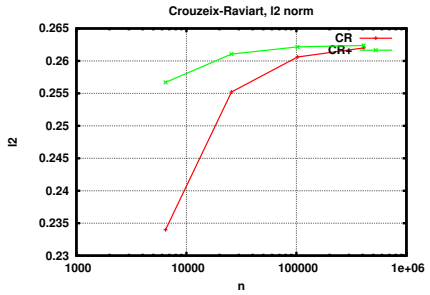

Figure 14: Problem 4, $\nu = 10^{-2}$: L^2 norm of the driven cavity velocity solution. n denotes the number of degrees of freedom

flow solution in Fig. 13 seems to compare well to typical results obtained by several authors, e.g., [29]. Also, the the computed L^2 norm of the numerical solution (≈ 0.262) compares well to the value obtained with a finite volume solver, and both numbers coincide in the first three leading decimal digits. Obviously, the convergence behaviour of the modified Crouzeix-Raviart scheme performs better than the classical scheme, see Tab. 12 and Tab. 13.

ndofs	$\|\mathbf{u}_h\|_0$
6,466	$2.3400054 \cdot 10^{-1}$
25,700	$2.5521782 \cdot 10^{-1}$
102,414	$2.6060792 \cdot 10^{-1}$
409,132	$2.6200594 \cdot 10^{-1}$

Table 12: Problem 4 (nonlinear), $\nu = 10^{-2}$: Numerical results for the classical Crouzeix-Raviart element

ndofs	$\|\mathbf{u}_h\|_0$
6,466	$2.5669241 \cdot 10^{-1}$
25,700	$2.6105730 \cdot 10^{-1}$
102,414	$2.6215868 \cdot 10^{-1}$
409,132	$2.6238548 \cdot 10^{-1}$

Table 13: Problem 4 (nonlinear), $\nu = 10^{-2}$: Numerical results for the classical Crouzeix-Raviart element

Acknowledgements

First, I want to thank Robert Eymard from the University Paris-Est for many stimulating discussions, his long-time encouragement, and for reading a preliminary note of this manuscript. Second, I want to thank Christian Brennecke from the Free University of Berlin, who implemented in his nice bachelor thesis project *Eine divergenzfreie Rekonstruktion für eine nichtkonforme Diskretisierung der inkompressiblen Stokes-Gleichungen*[7] the discretization approach described above for the first time (on two-dimensional structured grids for the incompressible Stokes equations). There, he received very encouraging numerical results comparing the classical Crouzeix-Raviart element with the modified one.

[1] G. Acosta, T. Apel, R. G. Durán, and A. L. Lombardi. Error estimates for Raviart-Thomas interpolation of any order on anisotropic tetrahedra. *Math. Comp.*, 80(273):141–163, 2011.

[2] G. Acosta and R. G. Durán. The maximum angle condition for mixed and nonconforming elements: application to the Stokes equations. *SIAM J. Numer. Anal.*, 37(1):18–36 (electronic), 1999.

[3] T. Apel, S. Nicaise, and J. Schöberl. A non-conforming finite element method with anisotropic mesh grading for the Stokes problem in domains with edges. *IMA J. Numer. Anal.*, 21(4):843–856, 2001.

[4] A. L. Bowers, B. R. Cousins, A. Linke, and L. G. Rebholz. New connections between finite element formulations of the Navier-Stokes equations. *J. Comput. Phys.*, 229(24):9020–9025, 2010.

[5] M. Braack, E. Burman, V. John, and G. Lube. Stabilized finite element methods for the generalized Oseen problem. *Comp. Meth. Appl. Mech. Engrg.*, 196(4–6):853–866, 2007.

[6] J. H. Brandts. Superconvergence and a posteriori error estimation for triangular mixed finite elements. *Numer. Math.*, 68(3):311–324, 1994.

[7] C. Brennecke. Eine divergenzfreie Rekonstruktion für eine nichtkonforme Diskretisierung der inkompressiblen Stokes-Gleichungen. Bachelor's thesis, Departement of Mathematics and Computer Science, Free University of Berlin, May 2013.

[8] F. Brezzi and M. Fortin. *Mixed and Hybrid Finite Elements*, volume 15 of *Springer Series in Computational Mathematics*. Springer, 1991.

[9] E. Burman and A. Linke. Stabilized finite element schemes for incompressible flow using Scott-Vogelius elements. *Appl. Numer. Math.*, 58(11):1704–1719, 2008.

[10] M. A. Case, V. J. Ervin, A. Linke, and L. G. Rebholz. A connection between Scott-Vogelius and grad-div stabilized Taylor-Hood FE approximations of the Navier-Stokes equations. *SIAM J. Numer. Anal.*, 49(4):1461–1481, 2011.

[11] B. Cockburn, G. Kanschat, and D. Schötzau. A locally conservative LDG method for the incompressible Navier-Stokes equations. *Math. Comp.*, 74(251):1067–1095 (electronic), 2005.

[12] B. Cockburn, G. Kanschat, and D. Schötzau. A note on discontinuous Galerkin divergence-free solutions of the Navier-Stokes equations. *J. Sci. Comput.*, 31(1-2):61–73, 2007.

[13] R. Codina. Numerical solution of the incompressible Navier-Stokes equations with Coriolis forces based on the discretization of the total time derivative. *J. Comput. Phys.*, 148(2):467–496, 1999.

[14] R. Codina and O. Soto. Finite element solution of the Stokes problem with dominating Coriolis force. *Comput. Methods Appl. Mech. Engrg.*, 142(3-4):215–234, 1997.

[15] M. Crouzeix and P.-A. Raviart. Conforming and nonconforming finite element methods for solving the stationary Stokes equations. I. *Rev. Française Automat. Informat. Recherche Opérationnelle Sér. Rouge*, 7(R-3):33–75, 1973.

[16] D. A. Di Pietro and A. Ern. *Mathematical aspects of discontinuous Galerkin methods*, volume 69 of *Mathématiques & Applications (Berlin) [Mathematics & Applications]*. Springer, Heidelberg, 2012.

[17] O. Dorok, W. Grambow, and L. Tobiska. Aspects of finite element discretizations for solving the Boussinesq approximation of the Navier-Stokes Equations. *Notes on Numerical Fluid Mechanics: Numerical Methods for the Navier-Stokes Equations. Proceedings of the International Workshop held at Heidelberg, October 1993, ed. by F.-K. Hebeker, R. Rannacher and G. Wittum*, 47:50–61, 1994.

[18] H. Elman, D. Silvester, and A. Wathen. *Finite Elements and Fast Iterative Solvers with applications in incompressible fluid dynamics*. Numerical Mathematics and Scientific Computation. Oxford University Press, Oxford, 2005.

[19] A. Ern and J. L. Guermond. *Theory and Practice of Finite Elements*, volume 159 of *Applied Mathematical Sciences*. Springer-Verlag, New York, 2004.

[20] J. A. Evans. *Divergence-free B-spline Discretizations for Viscous Incompressible Flows*. PhD thesis, University of Texas at Austin, 2011.

[21] J. A. Evans and T. J. R. Hughes. Isogeometric divergence-conforming B-splines for the steady Navier-Stokes equations. *Mathematical Models and Methods in Applied Sciences*, 23(08):1421–1478, 2013.

[22] R. S. Falk and M. Neilan. Stokes Complexes and the Construction of Stable Finite Elements with Pointwise Mass Conservation. *SIAM J. Numer. Anal.*, 51(2):1308–1326, 2013.

[23] L. P. Franca and T. J. R. Hughes. Two classes of mixed finite element methods. *Comput. Methods Appl. Mech. Engrg.*, 69(1):89–129, 1988.

[24] P. Frolkovic. Consistent velocity approximation for density driven flow and transport. In *Advanced Computational Methods in Engineering, Part 2*, pages 603–611, 1998.

[25] K. J. Galvin, A. Linke, L. G. Rebholz, and N. E. Wilson. Stabilizing poor mass conservation in incompressible flow problems with large irrotational forcing and application to thermal convection. *Comput. Methods Appl. Mech. Engrg.*, 237/240:166–176, 2012.

[26] S. Ganesan and V. John. Pressure separation — a technique for improving the velocity error in finite element discretisations of the Navier-Stokes equations. *Appl. Math. Comp.*, 165(2):275–290, 2005.

[27] T. Gelhard, G. Lube, M. Olshanskii, and J. Starcke. Stabilized finite element schemes with LBB-stable elements for incompressible flows. *J. Comput. Math.*, 177:243–267, 2005.

[28] J.-F. Gerbeau, C. Le Bris, and M. Bercovier. Spurious velocities in the steady flow of an incompressible fluid subjected to external forces. *International Journal for Numerical Methods in Fluids*, 25(6):679–695, 1997.

[29] U. Ghia, K. N. Ghia, and C. T. Shin. High-Re solutions for incompressible flow using the Navier-Stokes equations and a multigrid method. *J. Comput. Phys.*, 48:387–411, 1982.

[30] V. Girault and P.-A. Raviart. *Finite Element Methods for Navier-Stokes Equations*, volume 5 of *Springer Series in Computational Mathematics*. Springer-Verlag, Berlin, 1986.

[31] M. D. Gunzburger. The inf-sup condition in mixed finite element methods with application to the Stokes system. In *Collected lectures on the preservation of stability under discretization*, pages 93–121. SIAM, Fort Collins, 2002.

[32] E. Jenkins, V. John, A. Linke, and L. G. Rebholz. On the parameter choice in grad-div stabilization for incompressible flow problems. Technical Report 1751, WIAS, Berlin, 2012.

[33] W. Layton. *Introduction to the numerical analysis of incompressible viscous flows*, volume 6 of *Computational Science & Engineering*. Society for Industrial and Applied Mathematics (SIAM), Philadelphia, PA, 2008. With a foreword by Max Gunzburger.

[34] W. Layton, C. C. Manica, M. Neda, M. Olshanskii, and L. G. Rebholz. On the accuracy of the rotation form in simulations of the Navier-Stokes equations. *J. Comput. Phys.*, 228(9):3433–3447, 2009.

[35] A. Linke. *Divergence-free mixed finite elements for the incompressible Navier-Stokes Equation*. PhD thesis, University of Erlangen, 2008.

[36] A. Linke. Collision in a cross-shaped domain — a steady 2d Navier-Stokes example demonstrating the importance of mass conservation in CFD. *Computer Methods in Applied Mechanics and Engineering*, 198(41–44):3278–3286, 2009.

[37] A. Linke. A divergence-free velocity reconstruction for incompressible flows. *C. R. Math. Acad. Sci. Paris*, 350(17-18):837–840, 2012.

[38] A. Linke, L. G. Rebholz, and N. E. Wilson. On the convergence rate of grad-div stabilized Taylor-Hood to Scott-Vogelius solutions for incompressible flow problems. *J. Math. Anal. Appl.*, 381(2):612–626, 2011.

[39] M. Olshanskii, G. Lube, T. Heister, and J. Löwe. Grad-div stabilization and subgrid pressure models for the incompressible Navier-Stokes equations. *Comput. Methods Appl. Mech. Engrg.*, 198(49-52):3975–3988, 2009.

[40] M. Olshanskii and A. Reusken. Grad-div stabilization for Stokes equations. *Math. Comp.*, 73(248):1699–1718, 2004.

[41] J. Qin. *On the convergence of some low order mixed finite elements for incompressible fluids.* PhD thesis, Pennsylvania State University, 1994.

[42] P.-A. Raviart and J. M. Thomas. A mixed finite element method for 2nd order elliptic problems. In *Mathematical aspects of finite element methods (Proc. Conf., Consiglio Naz. delle Ricerche (C.N.R.), Rome, 1975)*, pages 292–315. Lecture Notes in Math., Vol. 606. Springer, Berlin, 1977.

[43] H.-G. Roos, M. Stynes, and L. Tobiska. *Robust numerical methods for singularly perturbed differential equations*, volume 24 of *Springer Series in Computational Mathematics*. Springer, Berlin, 2nd edition, 2008.

[44] J. R. Shewchuk. Triangle: Engineering a 2D Quality Mesh Generator and Delaunay Triangulator. In Ming C. Lin and Dinesh Manocha, editors, *Applied Computational Geometry: Towards Geometric Engineering*, volume 1148 of *Lecture Notes in Computer Science*, pages 203–222. Springer-Verlag, May 1996. From the First ACM Workshop on Applied Computational Geometry.

[45] H. Sohr. *The Navier-Stokes equations.* Modern Birkhäuser Classics. Birkhäuser/Springer Basel AG, Basel, 2001. An elementary functional analytic approach, [2013 reprint of the 2001 original] [MR1928881].

[46] R. Temam. *Navier-Stokes equations.* Elsevier, North-Holland, 1991.

[47] S. Turek, A. Ouazzi, and J. Hron. On pressure separation algorithms (PSepA) for improving the accuracy of incompressible flow simulations. *Internat. J. Numer. Methods Fluids*, 59(4):387–403, 2009.

[48] M. Vogelius. An analysis of the p-version of the finite element method for nearly incompressible materials. uniformly valid, optimal error estimates. *Numer. Math.*, 41:39–53, 1983.

[49] M. Vogelius. A right-inverse for the divergence operator in spaces of piecewise polynomials. Application to the p-version of the finite element method. *Numer. Math.*, 41:19–37, 1983.

[50] Junping Wang and Xiu Ye. New finite element methods in computational fluid dynamics by $H(\mathrm{div})$ elements. *SIAM J. Numer. Anal.*, 45(3):1269–1286 (electronic), 2007.

[51] S. Zhang. A new family of stable mixed finite elements for the 3d Stokes equations. *Math. Comp.*, 74(250):543–554, 2005.